Atmos. Chem. Phys. Discuss., https://doi.org/10.5194/acp-2019-26
Manuscript under review for journal Atmos. Chem. Phys.
Discussion started: 5 February 2019

Atmospheric Chemistry and Physics Discussions

Cloud macro-physical properties in Saharan dust laden and dust free North Atlantic trade wind regimes: A lidar study

Manuel Gutleben[1], Silke Groß[1], and Martin Wirth[1]

[1]Institut für Physik der Atmosphäre, Deutsches Zentrum für Luft- und Raumfahrt (DLR), 82234 Weßling, Germany.

Correspondence: Manuel Gutleben (manuel.gutleben@dlr.de)

Abstract. Saharan dust is known to have an important impact on the atmospheric radiation budget, both directly and indirectly by changing cloud properties. However, up to now it is still an open question if elevated and long-range transported Saharan dust layers have an effect on subjacent marine trade wind cloud occurrence. Shallow trade wind clouds have a significant impact on the Earth's radiation budget and still introduce large uncertainties in climate sensitivity estimates, because of their poor representation in climate models. The Next-generation Aircraft Remote-Sensing for Validation studies (NARVAL) aimed at providing a better understanding of shallow marine trade wind clouds and their interplay with long-range transported elevated Saharan dust layers. Two airborne campaigns were conducted - the first one in December 2013 and the second one in August 2016; the latter one during the peak season of transatlantic Saharan dust transport. Airborne lidar measurements in the vicinity of Barbados performed during the second field campaign are used to investigate possible differences between shallow marine cloud macro-physical properties in dust-free regions and regions comprising elevated Saharan dust layers. The cloud top height distribution derived in dust-laden regions differs from the one derived in dust-free regions and indicates that clouds are shallower and convective development is suppressed. Furthermore, regions comprising elevated Saharan dust layers show a larger fraction of small clouds and larger cloud free regions, compared to dust-free regions. The cloud fraction in dusty regions is only $14\,\%$ compared to a fraction of $31\,\%$ in dust-free regions. Moreover, a decreasing trend of cloud fractions and cloud top heights with increasing dust layer vertical extent as well as aerosol optical depth is found.

1 Introduction

Saharan dust represents one of the main contributors to the atmospheres primary aerosol load. Huneeus et al. (2011) estimate that every year 400 to $1000\,\mathrm{Tg}$ of Saharan mineral dust are mobilized and transported over the North Atlantic Ocean within an elevated atmospheric layer: the so-called Saharan air layer (SAL; Carlson and Prospero (1972), Prospero and Carlson (1972)). Transatlantic Saharan dust transport shows its maximum during the northern hemispheric summer (Prospero and Lamb, 2003). In this period dust particles are frequently transported westwards and arrive in the Caribbean after approximately 5 days (transport speed: $\sim 1000\,\mathrm{km\,d^{-1}}$ (Huang et al., 2010)). Sometimes Saharan dust is even transported as far as the coast of Mexico and Florida (Colarco (2003); Wong et al. (2006)). During its long-range transport the SAL affects the Earth's radiation budget in two different ways. On the one hand, the direct dust radiative effect modifies atmospheric stability, sea surface temperature and hence cloud development (Carlson and Benjamin (1980); Wong and Dessler (2005); Lau and Kim (2007)). On the other

Atmos. Chem. Phys. Discuss., https://doi.org/10.5194/acp-2019-26
Manuscript under review for journal Atmos. Chem. Phys.
Discussion started: 5 February 2019

hand, cloud lifetime and occurrence as well as precipitation and ice formation may be manipulated by Saharan dust deposition into the cloud layer (Mahowald and Kiehl (2003), Seifert et al. (2010)).

A theoretical study by Wong and Dessler (2005) suggests a possible suppressing effect of the SAL on deep convection, by showing that the convection barrier increases with SAL optical depth, especially over the eastern North Atlantic Ocean. They argue that the warmer and dryer air associated with the SAL rises the lifting condensation level as well as the level of free convection and therefore increases the energetic barrier to convection. As a result, the occurrence of deep convection is reduced. These findings also suggest a suppression of shallow marine cloud development due to long-range transported Saharan dust. However, observations of suppressed marine cloudiness underneath long-range transported layers of Saharan dust over the Atlantic Ocean are missing so far.

A large number of field campaigns aimed at getting a better understanding of the SAL as well as its interaction with clouds. The most extensive measurement series has probably been performed within the Saharan Mineral Dust Experiment series SAMUM-1 (Heintzenberg, 2009) and SAMUM-2 (Ansmann et al., 2011) followed by the Saharan Aerosol Long-range Transport and Aerosol-Cloud-Interaction Experiment (SALTRACE, Weinzierl et al. (2017)). Within this series of closure experiments, including airborne and ground-based in-situ and remote sensing measurements as well as modeling efforts, microphysical, chemical and radiative properties of dust were investigated at the beginning of its long-range transport near dust source regions as well as after its long-range transport in the vicinity of Barbados. Although the interaction of Saharan dust layers and clouds has already been a focus during these campaigns, e.g. by investigating glaciation of mixed-phase clouds (Ansmann et al., 2008; Seifert et al., 2010), the impact of long-range transported Saharan dust on subjacent trade wind cloud development has not been studied.

Due to their occurrence in remote locations over the subtropical North Atlantic Ocean, it is difficult to study undisturbed trade wind cloud regimes and Saharan air layers in the course of field campaigns with limited spatial coverage. Satellite measurements can of course provide information in these regions. Dunion and Velden (2004) used Geostationary Operational Environmental Satellite (GOES) infrared imagery to study the structural and dynamical characteristics of the SAL. They also suggest convective inhibition and associated reduction of deep convection due to the elevated SAL. Satellites with an active remote sensing payload, e.g. the Cloud-Aerosol Lidar and Infrared Pathfinder Satellite Observation (CALIPSO; (Winker et al., 2010)) and CloudSat (Stephens et al., 2002) additionally provide vertically highly resolved measurements of aerosol and cloud properties with nearly global coverage (Liu et al., 2008; Medeiros et al., 2010). However up to now, studies based on active remote-sensing satellite data with focus on cloud macro-physical properties concentrated on long-term and large-scale observations, e.g. low-latitude boundary layer cloud cover (Medeiros et al., 2010). From these observations it is also hard to get an accurate aerosol retrieval during daylight conditions, which makes it difficult to study the interplay of SAL and clouds.

Besides satellite observations, measurements from long range research aircraft provide a valuable alternative to study the problem at hand. One such platform is the German High Altitude and LOng range research aircraft HALO (Krautstrunk and Giez, 2012). With HALO it is possible to perform measurements over both SAL-influenced and clear regions within the very same flight. During the NARVAL-II field campaign (Next-generation Aircraft Remote-Sensing for Validation Studies-II) HALO was used as a flying aerosol and cloud observatory (Stevens et al., 2018, submitted). For this purpose it was equipped with a

Atmos. Chem. Phys. Discuss., https://doi.org/10.5194/acp-2019-26
Manuscript under review for journal Atmos. Chem. Phys.
Discussion started: 5 February 2019

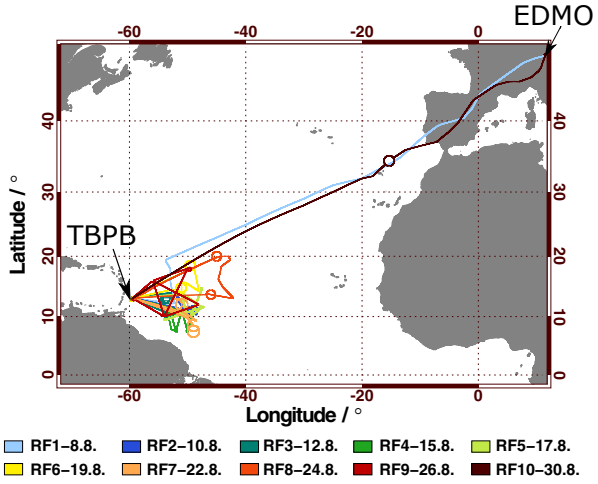

Figure 1. NARVAL-II research flight tracks (color coded with date information). Arrows indicate the locations of Grantley Adams International Airport (TBPB) and Airport Oberpfaffenhofen (EDMO).

combined active and passive remote sensing payload, including radar and lidar systems - probably the two most important instruments for vertically highly resolved measurements of aerosol and cloud properties. In addition, dropsondes were deployed to get information on the thermodynamic state of the atmosphere. This study is focused on the retrieval of horizontal and vertical distributions of both aerosols and clouds (i.e. cloud top height, cloud length) from lidar measurements performed in the course of NARVAL-II.

Chapter 2 gives an overview of the NARVAL-II field campaign and a description of the used lidar instrument. In Chapter 3 the general measurement situation during NARVAL-II is discussed and a detailed overview of the results is given. A short summary along with the conclusion of this paper is presented in Chapter 4.

2 Instruments and methods

2.1 NARVAL-II

In summer 2016 the Next-generation Aircraft Remote-Sensing for Validation Studies-II (NARVAL-II; Stevens et al. (2018, submitted)) were conducted to study the occurrence and formation of marine clouds during the subtropical North Atlantic wet season. As Saharan dust transportation over the Atlantic Ocean occurs quite frequently in northern hemispheric summer months, measurements were also dedicated to investigate the influence of the SAL on underlying shallow trade wind clouds.

During NARVAL-II, HALO was operated out of Barbados. The aircraft has a maximum range of more than $12\,000\,\mathrm{km}$ and a maximum cruising altitude of $\sim 15.5\,\mathrm{km}$. It was equipped with a combined active and passive remote sensing payload including the lidar system WALES (Wirth et al., 2009), a $35.2\,\mathrm{GHz}$ cloud radar (Ewald et al., 2018, in discussion), microwave radiometers (Mech et al., 2014), a hyper spectral imager (Ewald et al., 2016), and the SMART instrument for radiation measurements

Atmos. Chem. Phys. Discuss., https://doi.org/10.5194/acp-2019-26
Manuscript under review for journal Atmos. Chem. Phys.
Discussion started: 5 February 2019

Atmospheric Chemistry and Physics Discussions

Table 1. Overview of the conducted research flights during NARVAL-II in 2016 including dates, times of take-off and landing as well as research objectives and flight hours in SAL regions (all times given in UTC - note: Atlantic Standard Time = UTC-4; TBPB: Grantley Adams International Airport; EDMO: Airport Oberpfaffenhofen).

Flight No.	Date	Take-off [UTC]	Landing [UTC]	Research objective	Dust
RF1	08 Aug	08:12 (EDMO)	18:51 (TBPB)	Transfer flight	-
RF2	10 Aug	11:52 (TBPB)	20:02 (TBPB)	Dust/no dust flight	~ 2.3 h
RF3	12 Aug	11:43 (TBPB)	19:37 (TBPB)	Dust flight	~ 6.5 h
RF4	15 Aug	11:47 (TBPB)	19:46 (TBPB)	Dust/no dust flight	~ 2.7 h
RF5	17 Aug	14:47 (TBPB)	23:08 (TBPB)	Satellite validation	-
RF6	19 Aug	12:28 (TBPB)	20:52 (TBPB)	Dust/no dust flight	~ 4.5 h
RF7	22 Aug	13:16 (TBPB)	20:57 (TBPB)	ITCZ measurements	-
RF8	24 Aug	12:43 (TBPB)	20:55 (TBPB)	Tropical storm Garcon	-
RF9	26 Aug	13:43 (TBPB)	20:54 (TBPB)	Tropical storm Garcon	-
RF10	30 Aug	09:42 (TBPB)	19:52 (EDMO)	Transfer flight	-

(Wendisch et al., 2001). Additionally a large number of dropsondes were deployed to get information on the atmospheric state. From 8 to 30 August 2018, 10 research flights (RF) comprising a total of 85 flight hours were conducted (Figure 1). During four of those flights, flight patterns were specifically designed for an investigation of Saharan air layers and their impact on subjacent marine trade wind cloud regimes. Table 1 gives a detailed overview of all performed research flights including main research objectives.

This study focuses on the dust-laden RF2 to RF4 and RF6. A 22 h-lidar data set measured in the dust-free trades and a 16 h-lidar data set measured in SAL trade wind regions is used to study differences in macro-physical cloud properties in the respective regions during NARVAL-II.

2.2 The WALES instrument

The WALES instrument (Wirth et al., 2009) is a combined airborne high spectral resolution (HSRL; Esselborn et al. (2008)) and water vapor differential absorption lidar system (DIAL), built and operated by the Institute for Atmospheric Physics of the German Aerospace Center (DLR). The system provides highly resolved information on the vertical distribution of water vapor mixing ratio from measurements at four wavelengths around 935 nm. Additionally, it is capable of polarization sensitive measurements at 1064 nm and 532 nm wavelength. The 532 nm channel is also equipped with High Spectral Resolution Lidar (HSRL) capability, which allows to determine the extinction coefficient without assumption on scattering properties of aerosol and cloud particles, hence enabling an enhanced characterization of them.

WALES measurements are performed in near nadir direction (2° - 3° off-nadir angle) and provide vertical profiles of particle

Atmos. Chem. Phys. Discuss., https://doi.org/10.5194/acp-2019-26
Manuscript under review for journal Atmos. Chem. Phys.
Discussion started: 5 February 2019

Atmospheric Chemistry and Physics Discussions

backscatter, linear depolarization and extinction from the aircraft down to the ground level. The vertical resolution of the WALES aerosol and cloud data is $15\,\mathrm{m}$. The temporal resolution can be adjusted to suit the measurement situation. For the present study a temporal resolution of $1\,\mathrm{Hz}$, resulting in a horizontal resolution of approximately $200\,\mathrm{m}$ at typical aircraft speed, is used.

Depolarization data quality is ensured by frequent calibrations following to the $\pm 45°$ method described by Freudenthaler et al. (2009). Remaining relative uncertainties in aerosol depolarization measurements in the range from 10 to $16\,\%$ are primarily caused by the mechanical imprecision of the calibration setup (Esselborn et al., 2008) and possible atmospheric variations during the calibration. For backscatter and extinction measurements relative uncertainties of less than $5\,\%$ and 10 to $20\,\%$ have to be considered.

2.3 Dust layer detection

Based on the aerosol classification scheme described by Groß et al. (2013), WALES measurements can be used to identify and characterize layers of long-range transported Saharan dust. In this study the particle linear depolarization ratio at $532\,\mathrm{nm}$ (δ_{p532}) is used as an indicator for non-spherical dust particles. Saharan dust δ_{p532} near source regions was found to take values around $30\,\%$ (Freudenthaler et al., 2009; Tesche et al., 2009; Groß et al., 2011). This value does not change for long-range transported Saharan dust (Wiegner et al., 2011; Burton et al., 2015; Groß et al., 2015; Haarig et al., 2017). Thus δ_{p532} is a good proxy to distinguish long-range transported Saharan dust from less depolarizing marine boundary layer aerosols which typically take values around $3\,\%$ (Sakai et al., 2010; Burton et al., 2012; Groß et al., 2013). To reduce signal noise biases, an additional filter to flag mineral dust layers for regions with $532\,\mathrm{nm}$-backscatter ratios (BSR_{532}) equal or higher 1.2 is applied ($BSR_{532} = 1 + \beta_{p532}/\beta_{m532}$ - where β_{p532} and β_{m532} are the particle and molecular backscatter coefficients). The origin of identified dust layers is further verified using calculated backward trajectories utilizing the HYbrid Single Particle Lagrangian Integrated Trajectory model (HYSPLIT model, Stein et al. (2015)) with NCEP GDAS (National Centers for Environmental Prediction Global Data Assimilation System) data input. Starting times and locations are chosen accordingly to match the center of detected mineral dust layers in the lidar profiles. To check the reliability of the backward trajectory calculations, starting times and locations are slightly modified and results are compared.

Once verified as transported Saharan dust layer, the WALES HSRL particle extinction measurements at $532\,\mathrm{nm}$ are used to calculate the aerosol optical depth of both the detected Saharan dust layers ($\tau_{SAL(532)}$) and the atmospheric column ranging from the aircraft down to ground level ($\tau_{tot(532)}$). Additionally, the Saharan dust layer's vertical extent Δz_{SAL} is defined as the sum of all dust-flagged $15\,\mathrm{m}$-resolved height intervals within each vertical lidar profile.

2.4 Lidar-derived cloud macro-physical properties

Lidar derived cloud detection is usually performed using fixed signal thresholds (e.g. Medeiros et al. (2010); Nuijens et al. (2009, 2014)) or by applying wavelet covariance methods for the detection of sharp gradients to the backscattered signal (Gamage and Hagelberg, 1993). During NARVAL-II it was found that BSR_{532} in the cloud-free marine trade wind boundary layer as well as in the elevated SAL never exceeds a ratio of 10. Marine trade wind water-clouds are optically thick and thus

Atmos. Chem. Phys. Discuss., https://doi.org/10.5194/acp-2019-26
Manuscript under review for journal Atmos. Chem. Phys.
Discussion started: 5 February 2019

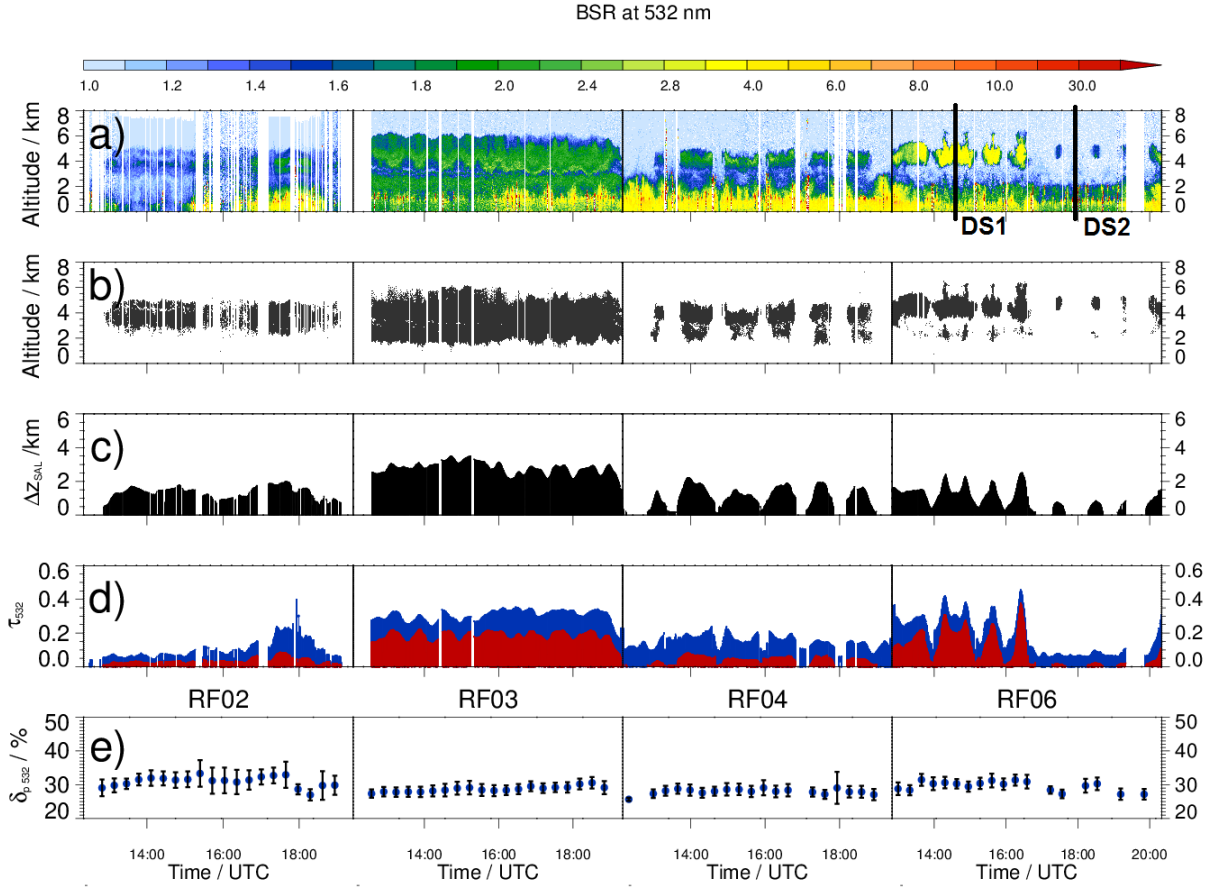

Figure 2. Overview of the four NARVAL-II research flights leading over Saharan dust-laden trade wind regions. (a) Cross sections of measured BSR at 532 nm and (b) applied mineral dust mask. Locations of dropsonde profiles discussed in section 3.2 are marked with black lines (DS1, DS2). (c) 10-minute boxcar average of the calculated dust layer vertical extent Δz_{SAL}. (d) 10-minute boxcar average of the derived total dust aerosol optical depth from aircraft to ground level $\tau_{tot(532)}$ (blue) and aerosol layer optical depth $\tau_{SAL(532)}$ (red). (e) Mean values and standard deviations of the measured 10-minute averaged SAL particle linear depolarization ratio (δ_{p532}).

take much larger values. Based on these findings and to avoid potential miscategorizations of sharp aerosol gradients as cloud tops using wavelet transforms a fixed threshold of $BSR_{532} = 20$ is used for the cloud/no-cloud decision.

To determine the cloud top height (CTH) in a vertical lidar profile the BSR_{532} profile is scanned from flight level downwards and the first range bin where BSR_{532} is greater or equal to the defined threshold is marked. Additionally, the whole profile is flagged as a 'cloud containing' profile. All 'cloud containing' profiles with cloud top heights in a certain altitude range are taken and divided by the total number of cloud-flagged profiles to obtain the CTH-fraction in the respective bin of the overall CTH-distribution. Similar to that the cloud fraction (CF) is defined as the number of all 'cloud containing' profiles divided by the total number of vertical lidar profiles.

Atmos. Chem. Phys. Discuss., https://doi.org/10.5194/acp-2019-26
Manuscript under review for journal Atmos. Chem. Phys.
Discussion started: 5 February 2019

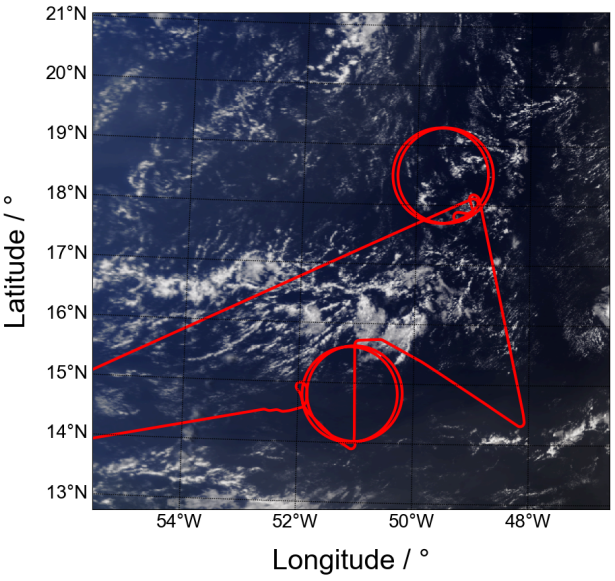

Figure 3. Flighttrack of RF6 on 19 Aug 2016 on top of a true color Terra-MODIS (MODerate-resolution Imaging Spectroradiometer) image taken at 13:40 UTC.

For the calculation of cloud lengths along the flight path neighboring cloud-flagged vertical profiles are connected and the cloud length is defined as the length of such a connected component. Cloud gaps are calculated analogously by connecting neighboring cloud-free profiles. It should be mentioned that not the maximum cloud (gap) length of each individual cloud, but the along-track cloud (gap) length is derived. As a result, the amount of small clouds (gaps) in this study may be overestimated.

3 Results

3.1 Dust measurements during NARVAL-II

In the following the measurement situation during the four HALO-flights used to characterize long-range transported Saharan dust layers (see Section 2.1) is summarized and their influence on subjacent marine trade wind clouds is investigated (Figure 4).

During RF2 on 10 August a thin Saharan dust layer ($\Delta z_{SAL} < 2\,\mathrm{km}$) ranging from 2.5 to $5.0\,\mathrm{km}$ altitude was detected during the whole flight. A mean δ_{p532} of $30\,\%$ clearly classifies this elevated layer as a mineral dust layer. $\tau_{SAL(532)}$ took values around 0.15 - on average approximately $35\,\%$ of the total column aerosol optical depth during this RF. Unfortunately, bright and strongly reflecting clouds in the lidar field of view caused the safety circuit of the detector unit to shut down the device, causing some gaps in the continuous lidar data set.

Atmos. Chem. Phys. Discuss., https://doi.org/10.5194/acp-2019-26
Manuscript under review for journal Atmos. Chem. Phys.
Discussion started: 5 February 2019

Atmospheric Chemistry and Physics Discussions

In contrast to RF2, a vertically and optically thick dust layer was observed during the whole RF3 on 12 August. δ_{p532} of this layer ranged from 28 to 30 %, thus confirming the presence of Saharan mineral dust. The layer had a maximum vertical extent of ∼4 km, showed aerosol optical depths around 0.2 and contributed on average with 60 % to the total column aerosol optical depth during that flight.

While RF2 and RF3 were designed for measurements solely in dust-laden regions, RF4 and RF6 on 15 and 19 August were planned for measurements in both dust-laden and dust-free regions within the very same research flight. Flight tracks were chosen to cross dust-gradients frequently, resulting in multiple flight segments of dust and no dust along the flight track. Elevated aerosol layers showed mean δ_{p532} of 30 % and could therefore be identified as SAL. While the SAL during RF4 ranged on average from 2.5 to 4.5 km, it reached higher to almost 6 km altitude during RF5. With $\tau_{SAL(532)} \approx 0.1$ the dust layer during RF4 contributed on average 25 % to $\tau_{tot(532)}$. $\tau_{SAL(532)}$ during RF6 took higher values of up to 0.4 and showed a mean contribution of 51 % to $\tau_{tot(532)}$.

The following case study presents a detailed description of RF6 including an analysis of dropsonde-profiles in dust laden and dust free regions.

3.2 Case study - 19 Aug 2016

RF6 on 19 August 2016 took place in the area between 48°W to 60°W and 13°N to 19°N (Figure 3). The Intertropical Convergence Zone (ITCZ) and associated deep convection were located far south of the flight track. Thus, it is not expected to have an influence of the ITCZ on our analysis. RF6 was planned to cross a sharp gradient between a dust-laden and a clear region in an altitude of approximately 8.25 km with about one half of the measurement time in dust-laden and the other half in dust-free regions. The circular patterns of the flight track were planned for dropsonde-based divergence measurements. Whereas the first pair of circles was performed over a heavily dust-laden region in the southern part of the flight track, the second pair was performed in the northern part over a dust-free region.

Measured cross sections of BSR_{532} and the derived mineral-dust mask (Figure 2 (a, RF6) and (b, RF6)) show pronounced elevated mineral dust layers ranging from 2.5 to 5.0 km altitude, horizontally alternating with dust-free profile regions. Backward trajectory calculations affirm the Saharan origin of the layers (not shown here). Dropsondes were launched frequently along the circular flight paths and are used to compare vertical profiles of meteorological parameters in dust-laden to those in dust-free regions. For this purpose two representative dropsonde measurements are selected: one in the southerly SAL-region (D1) and another one in the more northerly dust-free region (D2) where only some residual Saharan dust is detected. Additionally the lidar-derived δ_{p532} is analyzed at the locations of the dropped sondes (D1: 14.94° N, 51.866 E; D2: 17.755° N, 49.195° E).

Inside the SAL-region (D1) a three-layer structure is present: 1) the marine boundary layer (MBL), reaching up to approximately 1.3 km height. δ_{p532} smaller 10 % indicate that marine aerosols are the dominant contributor to the aerosol composition of the MBL; 2) a transition or mixed layer extending from the MBL-top to ∼2.5 km altitude with varying values of δ_{p532} (10 % < δ_{p532} < 20 %); and 3) the elevated SAL, with typical δ_{p532} for long-range transported Saharan dust (δ_{p532} ∼30 %) ranging from 2.8 to 4.0 km height.

The dust-free δ_{p532}-profile (D2) of the MBL and transition layer looks quite similar to dust-laden profile (D1). However, no

Atmos. Chem. Phys. Discuss., https://doi.org/10.5194/acp-2019-26
Manuscript under review for journal Atmos. Chem. Phys.
Discussion started: 5 February 2019

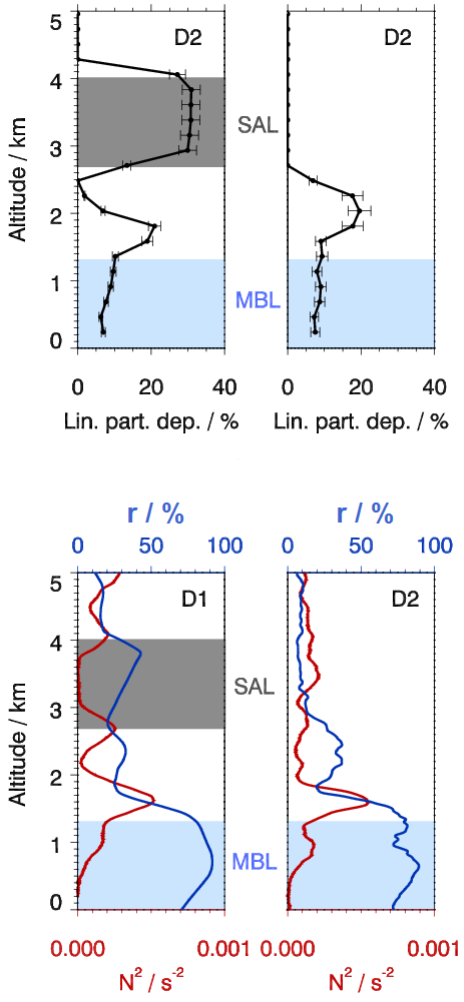

Figure 4. Dropsonde and lidar derived vertical profiles of δ_{p532} (error bars indicate systematic errors), relative humidity (r), and squared Brunt-Väisälä frequency $N^2 = \frac{g}{\Theta}\frac{d\Theta}{dz}$ at waypoints D1 (left panels) and D2 (right panels) - A running mean $\pm$ 150 m is applied to reveal general features in N^2-profiles.

SAL-signature is detected. The low CF in the dust-laden region (southern part of the flight track) which is visible in the MODIS image (Moderate-resolution Imaging Spectroradiometer; Figure 3) is also evident in lidar measurements after the application of the described threshold method for cloud detection. Whereas a lot of cloud tops in heights ranging from 0.5 to 1.5 km altitude are detected in the northern part of the flight track (after about 16:45 UTC), almost no cloud is detected along the earlier southern flight path - with the exception of the transition region to the dust free area (cloud top heights at ∼1.5 km altitude). This is also evident in the calculated cloud fractions. CF is 20 % in dust-free regions. In the SAL-region however, CF decreases to 11 % (including the clouds developing at the edges of the dust layer). Another characteristic of clouds in SAL-regions is

Atmos. Chem. Phys. Discuss., https://doi.org/10.5194/acp-2019-26
Manuscript under review for journal Atmos. Chem. Phys.
Discussion started: 5 February 2019

Atmospheric Chemistry and Physics Discussions

that their CTH is rarely higher than approximately 1 km. However, in dust free regions cloud top heights reach almost twice as high and up to 2 km.

Differences in meteorological parameters between SAL-regions and dust-free regions are discussed by looking at dropsonde measurements (D1, D2). Both dropsondes clearly indicate the so-called trade wind inversion (TWI) in the altitude range from 1.3 to 1.7 km height capping the moist MBL. The TWI is characterized by a rapid temperature increase of about 4 K within 400 m (not shown) and a strong hydrolapse (relative humidity (r) drops from >80 to ∼30 %). The MBL itself shows no significant variations in relative humidity in both the dust-free and the dust-laden regimes with mean values of 85 %. For a better visualisation of regions featuring high atmospheric stability the squared Brunt Väisälä frequency $N^2 = \frac{g}{\Theta}\frac{d\Theta}{dz}$, with g being the gravity of the Earth and Θ the potential temperature, is shown. N^2 shows regions of high atmospheric stability and thus strong restoring forces for a vertical air parcel displacement at the inversion altitudes. Enhanced atmopspheric stability is found at the TWI for both analyzed dropsonde measurements. At higher altitudes the N^2-profiles look different. In dust-laden regions the lower and upper boundary of the SAL are characterized by two additional well-known inversions (Carlson and Prospero, 1972; Dunion and Velden, 2004; Ismail et al., 2010). Altogether, a total of three prominent inversion layers counteract convective development in dust-laden regions, whereas in dust-free regions only the trade wind inversion is present.

3.3 Differences in cloud macro-physical properties

In a next step differences in macro-physical properties of shallow marine clouds between the identified dust-laden and dust-free flight segments are studied.

3.3.1 Cloud fraction and cloud top height

A fist indicator for differences in marine trade wind cloud occurrence is the cloud fraction CF. During NARVAL-II a total number of 3.2×10^4 one second resolved cloud tops were detected in trade wind regions ($N_{CT(dust)} = 8 \times 10^3$; $N_{CT(nodust)} = 2.4 \times 10^4$). They contribute to an overall observed CF of 24 % within the measurement period. In dust-free regions a CF of 31 % was derived, while in SAL-regions CF was smaller by a factor of more than two (14 %). The next parameter to look for differences between the two cases is the CTH-distribution for both regions (Figure 5). In the SAL-regions only a small fraction of clouds exceeds an altitude of 2 km and no cloud top is found at altitudes greater 2.5 km. The majority of cloud top heights (∼61 %) is found within the altitude range from 0.5 to 1.0 km. 26 % of all detected cloud top heights are located in the 1.0 to 1.5 km height interval and only 11 % of that fraction contribute to the interval from 1.5 to 2.0 km altitude. Cloud tops in altitudes >2.5 km including deeper reaching convection with maximum top heights of 6 km are found in ∼16 % of all dust-free cloud profiles. Underneath around 3 km altitude the CTH-distribution shows a two-modal structure with two local maxima ranging from 0.5 to 1.0 km (∼35 %) and 1.5 to 2.0 km altitude (∼20 %).

The statistical significance of observed differences in the distributions was checked by randomly resampling the respective data-sets to smaller sub-sets and by comparing the shapes of the resulting distributions to the shape of the overall distributions. The shapes of the resampled distributions showed no major differences compared to the overall distributions, thus it can be

Atmos. Chem. Phys. Discuss., https://doi.org/10.5194/acp-2019-26
Manuscript under review for journal Atmos. Chem. Phys.
Discussion started: 5 February 2019

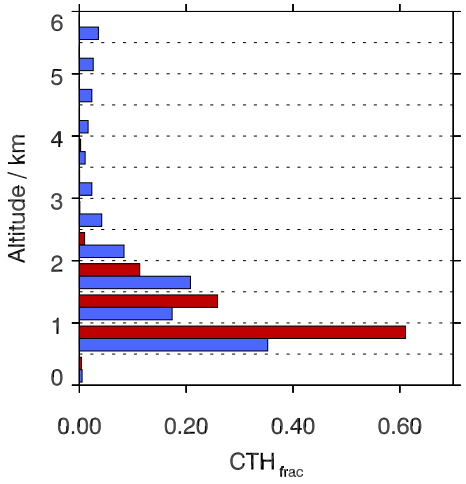

Figure 5. Histograms of detected cloud top height fractions during NARVAL-II with bins of $0.5\,\mathrm{km}$ size. Red bars illustrate the distribution of cloud tops height fractions in SAL-regions. Blue bars represent the derived cloud top height distribution from measurements in the dust-free trades.

concluded that our NARVAL-II measurements indicate the presence of less and shallower clouds in Saharan dust laden trade wind regions compared to dust-free regions.

3.3.2 Cloud lengths and cloud gaps

As next step the cloud length and cloud gap length distributions of marine trade wind clouds in SAL-regions and mineral dust free regions are investigated (Figure 6, top). A total of 3688 and 2355 clouds were observed in dust free and dust-laden regions during the NARVAL-II research flights. In both regions clouds with a horizontal extent of less than $0.5\,\mathrm{km}$ are by far the most prominent cloud type. Whereas $72\,\%$ of all clouds in SAL-regions are of this length, $65\,\%$ of all clouds detected in clear regions contribute to this length-interval. In both regions the frequency of cloud length occurrence decreases strongly with increasing cloud length. Relative frequency drops to $\sim 17\,\%$ (dust-laden) and $\sim 16\,\%$ (dust-free) in the length interval from 0.5 to $1.0\,\mathrm{km}$. Only $5\,\%$ of all clouds in dusty regions are observed to have a horizontal extent greater than $2\,\mathrm{km}$. This fraction almost doubles to $9\,\%$ in dust-free regions. The main contributor to this fraction are clouds with horizontal extents of more than $5\,\mathrm{km}$ ($4\,\%$). Clouds of this length are basically only found outside dust-laden regions.

Another important parameter to highlight differences of cloudiness between SAL-regions and dust-free regions is the cloud gap length (Figure 6, bottom). Similar to the distribution of cloud lengths, also cloud gap frequencies decrease with increasing cloud gap length. In both regimes cloud gaps shorter $0.5\,\mathrm{km}$ are dominating. They contribute with $45\,\%$ and $35\,\%$ to the total amount of observed cloud gaps in dust-free and dust-laden regions. A reverse picture emerges, when looking at the amount of cloud gaps greater than $5\,\mathrm{km}$. A fraction of $17\,\%$ is found to be greater than $5\,\mathrm{km}$ underneath dust layers, whereas in dust-free regions these gap sizes contribute with $12\,\%$ to the distribution. Cloud gap fractions in range-bins from 1.5 to $4.5\,\mathrm{km}$ decrease

Atmos. Chem. Phys. Discuss., https://doi.org/10.5194/acp-2019-26
Manuscript under review for journal Atmos. Chem. Phys.
Discussion started: 5 February 2019

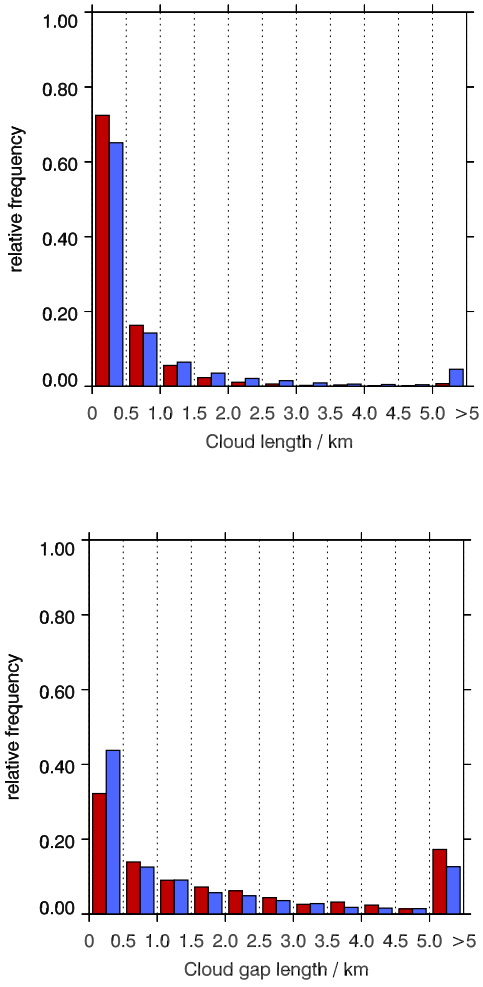

Figure 6. Histograms of detected cloud lengths (top) and cloud gap lengths (bottom). Red bars illustrate the distribution of marine low cloud (gap) lengths located underneath Saharan dust layers. Blue bars represent the cloud (gap) length distribution derived from measurements in dust-free areas.

Atmos. Chem. Phys. Discuss., https://doi.org/10.5194/acp-2019-26
Manuscript under review for journal Atmos. Chem. Phys.
Discussion started: 5 February 2019

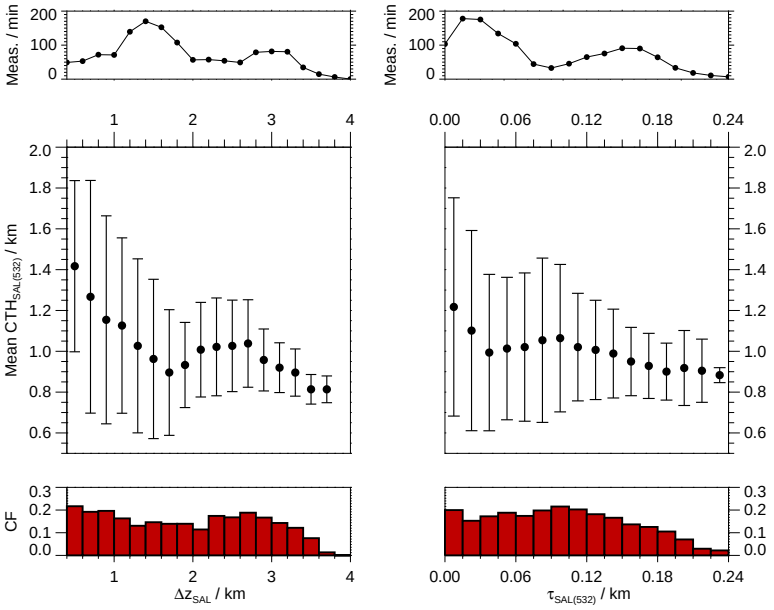

Figure 7. Left: Mean cloud top heights (middle) and cloud fraction (bottom) of clouds detected underneath Saharan dust layers as a function of Saharan dust layer vertical extent (Δz_{SAL}) - bin-interval: $0.2\,\mathrm{km}$, Right: Mean cloud top heights (middle) and cloud fraction (bottom) of clouds detected underneath Saharan dust layers as a function of Saharan dust layer optical depth ($\tau_{SAL(532)}$) at $532\,\mathrm{nm}$ wavelength - bin-interval: 0.015. Bars mark respective standard deviations of mean cloud top heights (1σ). The uppermost graphs illustrate summed measurement-times in each interval.

in both regions consistently with increasing cloud gap length.

The significance of the distribution-properties was again double-checked by the comparison to randomly resampled sub-datasets. Overall, the cloud length and gap length distributions (Figure 6) indicate, that the dust-laden trade wind regimes during NARVAL-II were characterized by a larger amount of small scale clouds and slightly greater cloud gaps, compared to the dust free regimes.

3.3.3 Connecting dust and cloud properties

As a further step the observed CTH and CF are related to the geometrical and optical depth (Δz_{SAL} and $\tau_{SAL(532)}$) of overlying mineral dust layers (Figure 7). Cloud fractions and heights in dust-flagged profiles of all four research flight are grouped together with respect to similar Δz_{SAL} (bin width: $0.2\,\mathrm{km}$) and $\tau_{SAL(532)}$ (bin width: 0.015). During NARVAL-II Saharan dust layers with maximum vertical extents of $4\,\mathrm{km}$ and maximum optical depths of 0.4 were observed (Figure 2). However, underneath optically thick dust layers ($0.24 < \tau_{SAL(532)}$; $3.8\,\mathrm{km} < \Delta z_{SAL}$) not any cloud has been detected.

The distribution of CTH as a function of Δz_{SAL} shows that up to a layer thickness of $1.6\,\mathrm{km}$ mean CTH decreases with increasing Δz_{SAL} from $\sim$1.4 to $\sim$0.8 km altitude. For a greater layer thickness (Δz_{SAL}>1.6 km) this trend is not evident

anymore. A further increase in Δz_{SAL} does not imply a significant decrease in mean CTH - in some bin-intervals the mean CTH even increases slightly. Mean cloud top heights vary strongly underneath vertically thin dust layers (σ = 0.5 km) - an indication for the presence of both shallow developing convective clouds and higher reaching trade wind clouds within the MBL. With increasing Δz_{SAL} the variability of mean CTH decreases and reduces to σ <0.2 km for Δz_{SAL} <3 km. This suggests that the cloud layer indeed lowers and that the few evolving clouds are confined to low levels of the MBL. The CF distribution as a function of Δz_{SAL} does not show any distinct trend for geometrically thin layers. For Δz_{SAL} <1.0 km CF takes values around 20 % - only slightly lower values than the CF derived from measurements in dust-free regions. For vertical extents ranging from 1.0 km < Δz_{SAL} < 2.6 km no clear decrease in CF is detected. In this range CF varies around 15 % and even increases slightly. A clear decreasing trend of CF with increasing Δz_{SAL} is obvious only for Δz_{SAL}>2.6 km.

Next, the CTH distribution as a function of dust layer optical depth $\tau_{SAL(532)}$ is analyzed. Up to a value of $\tau_{SAL(532)}$ ~0.05 the mean CTH decreases with increasing optical depth of the aerosol layer. The mean CTH drops from ~1.3 km to ~ 1.0 km in this region. A further increase of $\tau_{SAL(532)}$ to a value of about 0.12 does not show any further decrease in mean CTH. This is in line with the observed decrease in CF as a function of dust layer optical depth in this range. The observed CF increases slightly from 15 to 20 % for small SAL-optical depths ($\tau_{SAL(532)} < 0.12$). At the upper tail of the distribution ($0.12 < \tau_{SAL(532)}$) the mean CTH as well as the CF decrease again. CF shows a steady decrease of about 20 % in the range from $\tau_{SAL(532)}$ =0.12 to 0.24. Moreover, the variability of mean CTH in that range gets smaller, again indicating that higher-reaching convection is suppressed.

For the interpretation of these distributions the accumulated measurement-time in the respective intervals as well as the contribution of different research flights have to be taken into account. Mainly data collected in the course of RF3 contributes to SAL-measurements in the ranges 0.09< $\tau_{SAL(532)}$ <0.24 and 2 km< Δz_{SAL} <4 km (Figure 2), thus being the main contributor to observed increases of mean CTH and CF in regions of high $\tau_{SAL(532)}$ and Δz_{SAL}. The remaining research flights (RF2, RF4 and RF6), were characterized by thinner dust layers that were rather decoupled from the MBL and contribute to regions of small $\tau_{SAL(532)}$ and Δz_{SAL}.

Altogether, a decreasing trend of CTH and CF as a function of dust layer optical depth and vertical extent was detected during research flights over elevated and long-range transported Saharan dust layers. However, RF3 showed a predominant and strongly pronounced transition layer that possibly altered the cloud layer resulting in an increased CF and CTH in the respective intervals of $\tau_{SAL(532)}$ and Δz_{SAL}.

4 Summary and Conclusion

In this study airborne lidar measurements performed on-board the German high altitude and long-range research aircraft HALO during the NARVAL-II experiment over the North Atlantic trade wind region were used to investigate whether marine low cloud macro-physical properties change in the presence of overlying long-range transported Saharan dust layers. Significant differences in the CTH distribution as well as in the cloud length and cloud gap length distribution were found for flights in SAL-regions compared to the distributions derived from flights in dust-free regions. It can be summarized that dust-laden

regions implicate less, shallower and smaller clouds than dust-free regions. The overall derived cloud fraction in the dust-laden trades is $14\,\%$ and thus a factor of two smaller than the cloud fraction of $31\,\%$ derived from observations in the dust-free trades. These results are in good agreement with previous satellite remote sensing studies (Dunion and Velden, 2004) and model studies (Wong and Dessler, 2005; Stephens et al., 2004) which also suggest a convection-suppressing characteristic of the SAL with the main player being a dry anomaly in SAL-altitudes. During NARVAL-II long-range Saharan air layers were not found to come along with dry anomalies, but were rather showing enhanced relative humidities in the range from 30 to $40\,\%$. However, a suppressing characteristic of the SAL on subjacent marine clouds, is evident as well.

Wong and Dessler (2005) also showed that the convection barrier increases with SAL-aerosol optical depth. To investigate a possible relation between SAL optical depth or layer vertical extent and marine trade wind CTH, the CTH and CF-distribution was analyzed as a function of SAL vertical extent and optical depth. It was found that mean CTH decreases with increasing layer vertical extent for vertically thin layers ($<1.5\,\mathrm{km}$). Additionally, the mean CTH-variability for these layers is high, indicating the occurrence of higher-reaching clouds in those regions. There is no significant decrease of mean CTH for thicker dust layers, but a reduction of CTH-variability could be derived. Also a decrease in mean CTH-variability with increasing dust layer optical thickness starting at $\tau_{SAL(532)} \approx 1.2$ could be detected. This indicates that optically and vertically thicker dust layers suppress the evolution of higher reaching convection. Moreover, a decrease in CF comes along with this reduction in variability of the mean CTH. Underneath optically thick dust layers with $0.24 < \tau_{SAL(532)}$ not any cloud was detected.

Altogether, NARVAL-II lidar measurements indicate that there is a strong correlation between the presence of elevated and long-range transported Saharan dust layers and the occurrence and macro-physical properties of subjacent marine low clouds. Further reaching questions regarding changes in radiation caused by the dust layer, changes in the general circulation patterns or the settling of dust particles into the cloud layer (Groß et al., 2016) could not be addressed within the present work and are left to future studies.

Author contributions. In the framework of the NARVAL-II field experiment Martin Wirth and Silke Groß contributed to carry out all airborne lidar measurements used in this study. Martin Wirth did the initial data processing. Manuel Gutleben performed all analytic computations, statistically analyzed the data set and took the lead in writing the manuscript under consultation of Silke Groß. All authors discussed the results and contributed to the final manuscript.

Competing interests. none declared

Acknowledgements. The authors like to thank the staff members of the DLR HALO aircraft from DLR Flight Experiments for preparing and performing the measurement flights. Data sets used in this publication were collected during the NARVAL-II (Next-generation Aircraft Remote-Sensing for Validation Studies-II) campaign and are made available in the HALO Database. NARVAL-II was funded with support

of the Max Planck Society, the German Research Foundation (DFG) and the German Aerospace Center (DLR). This study was financed by a DLR VO-R young investigator group within the Institute of Atmospheric Physics.

References

Ansmann, A., Tesche, M., Althausen, D., Müller, D., Seifert, P., Freudenthaler, V., Heese, B., Wiegner, M., Pisani, G., Knippertz, P., and Dubovik, O.: Influence of Saharan dust on cloud glaciation in southern Morocco during the Saharan Mineral Dust Experiment, J. Geophys. Res., 113, https://doi.org/10.1029/2007jd008785, 2008.

Ansmann, A., Petzold, A., Kandler, K., Tegen, I., Wendisch, M., Müller, D., Weinzierl, B., Müller, T., and Heintzenberg, J.: Saharan Mineral Dust Experiments SAMUM–1 and SAMUM–2: what have we learned?, Tellus B, 63, 403–429, https://doi.org/10.1111/j.1600-0889.2011.00555.x, 2011.

Burton, S. P., Ferrare, R. A., Hostetler, C. A., Hair, J. W., Rogers, R. R., Obland, M. D., Butler, C. F., Cook, A. L., Harper, D. B., and Froyd, K. D.: Aerosol classification using airborne High Spectral Resolution Lidar measurements – methodology and examples, Atmos. Meas. Tech., 5, 73–98, https://doi.org/10.5194/amt-5-73-2012, 2012.

Burton, S. P., Hair, J. W., Kahnert, M., Ferrare, R. A., Hostetler, C. A., Cook, A. L., Harper, D. B., Berkoff, T. A., Seaman, S. T., Collins, J. E., Fenn, M. A., and Rogers, R. R.: Observations of the spectral dependence of linear particle depolarization ratio of aerosols using NASA Langley airborne High Spectral Resolution Lidar, Atmos. Chem. Phys., 15, 13 453–13 473, https://doi.org/10.5194/acp-15-13453-2015, 2015.

Carlson, T. N. and Benjamin, S. G.: Radiative heating rates for Saharan dust, J. Atmos. Sci., 37, 193–213, https://doi.org/10.1175/1520-0469(1980)037<0193:RHRFSD>2.0.CO;2, 1980.

Carlson, T. N. and Prospero, J. M.: The Large-Scale Movement of Saharan Air Outbreaks over the Northern Equatorial Atlantic, J. Appl. Meteorol., 11, 283–297, https://doi.org/10.1175/1520-0450(1972)011<0283:TLSMOS>2.0.CO;2, 1972.

Colarco, P. R.: Saharan dust transport to the Caribbean during PRIDE: 1. Influence of dust sources and removal mechanisms on the timing and magnitude of downwind aerosol optical depth events from simulations of in situ and remote sensing observations, J. Geophys. Res., 108, https://doi.org/10.1029/2002jd002658, 2003.

Dunion, J. P. and Velden, C. S.: The Impact of the Saharan Air Layer on Atlantic Tropical Cyclone Activity, B. Am. Meteorol. Soc., 85, 353–366, https://doi.org/10.1175/BAMS-85-3-353, 2004.

Esselborn, M., Wirth, M., Fix, A., Tesche, M., and Ehret, G.: Airborne high spectral resolution lidar for measuring aerosol extinction and backscatter coefficients, Appl. Opt., 47, 346–358, https://doi.org/10.1364/AO.47.000346, 2008.

Ewald, F., Kölling, T., Baumgartner, A., Zinner, T., and Mayer, B.: Design and characterization of specMACS, a multipurpose hyperspectral cloud and sky imager, Atmos. Meas. Tech., 9, 2015–2042, https://doi.org/10.5194/amt-9-2015-2016, 2016.

Ewald, F., Groß, S., Hagen, M., Hirsch, L., Delanoë, J., and Bauer-Pfundstein, M.: Calibration of a 35-GHz Airborne Cloud Radar: Lessons Learned and Intercomparisons with 94-GHz Cloud Radars, Atmos. Meas. Tech. Discuss., pp. 1–32, https://doi.org/10.5194/amt-2018-269, 2018, in discussion.

Freudenthaler, V., Esselborn, M., Wiegner, M., Heese, B., Tesche, M., Ansmann, A., Müller, D., Althausen, D., Wirth, M., Fix, A., Ehret, G., Knippertz, P., Toledano, C., Gasteiger, J., Garhammer, M., and Seefeldner, M.: Depolarization ratio profiling at several wavelengths in pure Saharan dust during SAMUM 2006, Tellus B, 61, 165–179, https://doi.org/10.1111/j.1600-0889.2008.00396.x, 2009.

Gamage, N. and Hagelberg, C.: Detection and Analysis of Microfronts and Associated Coherent Events Using Localized Transforms, J. Atmos. Sci, 50, 750–756, https://doi.org/10.1175/1520-0469(1993)050<0750:daaoma>2.0.co;2, 1993.

Groß, S., Wiegner, M., Freudenthaler, V., and Toledano, C.: Lidar ratio of Saharan dust over Cape Verde Islands: Assessment and error calculation, J. Geophys. Res. - Atmos, 116, https://doi.org/10.1029/2010JD015435, 2011.

Groß, S., Esselborn, M., Weinzierl, B., Wirth, M., Fix, A., and Petzold, A.: Aerosol classification by airborne high spectral resolution lidar observations, Atmos. Chem. Phys., 13, 2487–2505, https://doi.org/10.5194/acp-13-2487-2013, 2013.

Groß, S., Freudenthaler, V., Schepanski, K., Toledano, C., Schäfler, A., Ansmann, A., and Weinzierl, B.: Optical properties of long-range transported Saharan dust over Barbados as measured by dual-wavelength depolarization Raman lidar measurements, Atmos. Chem. Phys, 15, 11 067–11 080, https://doi.org/10.5194/acp-15-11067-2015, 2015.

Groß, S., Gasteiger, J., Freudenthaler, V., Müller, T., Sauer, D., Toledano, C., and Ansmann, A.: Saharan dust contribution to the Caribbean summertime boundary layer – a lidar study during SALTRACE, Atmos. Chem. Phys., 16, 11 535–11 546, https://doi.org/10.5194/acp-16-11535-2016, 2016.

Haarig, M., Ansmann, A., Althausen, D., Klepel, A., Groß, S., Freudenthaler, V., Toledano, C., Mamouri, R.-E., Farrell, D. A., Prescod, D. A., Marinou, E., Burton, S. P., Gasteiger, J., Engelmann, R., and Baars, H.: Triple-wavelength depolarization-ratio profiling of Saharan dust over Barbados during SALTRACE in 2013 and 2014, Atmos. Chem. Phys., 17, 10 767–10 794, https://doi.org/10.5194/acp-17-10767-2017, 2017.

Heintzenberg, J.: The SAMUM-1 experiment over Southern Morocco: overview and introduction, Tellus B, 61, 2–11, https://doi.org/10.1111/j.1600-0889.2008.00403.x, 2009.

Huang, J., Zhang, C., and Prospero, J. M.: African dust outbreaks: A satellite perspective of temporal and spatial variability over the tropical Atlantic Ocean, J. Geophys. Res. - Atmos, 115, https://doi.org/10.1029/2009JD012516, 2010.

Huneeus, N., Schulz, M., Balkanski, Y., Griesfeller, J., Prospero, J., Kinne, S., Bauer, S., Boucher, O., Chin, M., Dentener, F., Diehl, T., Easter, R., Fillmore, D., Ghan, S., Ginoux, P., Grini, A., Horowitz, L., Koch, D., Krol, M. C., Landing, W., Liu, X., Mahowald, N., Miller, R., Morcrette, J.-J., Myhre, G., Penner, J., Perlwitz, J., Stier, P., Takemura, T., and Zender, C. S.: Global dust model intercomparison in AeroCom phase I, Atmos. Chem. Phys., 11, 7781–7816, https://doi.org/10.5194/acp-11-7781-2011, 2011.

Ismail, S., Ferrare, R. A., Browell, E. V., Chen, G., Anderson, B., Kooi, S. A., Notari, A., Butler, C. F., Burton, S., Fenn, M., Dunion, J. P., Heymsfield, G., Krishnamurti, T. N., and Biswas, M. K.: LASE Measurements of Water Vapor, Aerosol, and Cloud Distributions in Saharan Air Layers and Tropical Disturbances, J. Atmos. Sci., 67, 1026–1047, https://doi.org/10.1175/2009JAS3136.1, 2010.

Krautstrunk, M. and Giez, A.: The Transition from FALCON to HALO Era Airborne Atmospheric Research, in: Atmospheric Physics, edited by Schumann, U., Research Topics in Aerospace, pp. 609–624, Springer Berlin Heidelberg, 2012.

Lau, K. M. and Kim, K. M.: Cooling of the Atlantic by Saharan dust, Geophys. Res. Lett., 34, https://doi.org/10.1029/2007GL031538, 2007.

Liu, Z., Omar, A., Vaughan, M., Hair, J., Kittaka, C., Hu, Y., Powell, K., Trepte, C., Winker, D., Hostetler, C., Ferrare, R., and Pierce, R.: CALIPSO lidar observations of the optical properties of Saharan dust: A case study of long-range transport, J. Geophys. Res. - Atmos, 113, https://doi.org/10.1029/2007JD008878, 2008.

Mahowald, N. M. and Kiehl, L. M.: Mineral aerosol and cloud interactions, Geophys. Res. Lett., 30, https://doi.org/10.1029/2002GL016762, 1475, 2003.

Mech, M., Orlandi, E., Crewell, S., Ament, F., Hirsch, L., Hagen, M., Peters, G., and Stevens, B.: HAMP – the microwave package on the High Altitude and LOng range research aircraft (HALO), Atmos. Meas. Tech., 7, 4539–4553, https://doi.org/10.5194/amt-7-4539-2014, 2014.

Medeiros, B., Nuijens, L., Antoniazzi, C., and Stevens, B.: Low-latitude boundary layer clouds as seen by CALIPSO, J. Geophys. Res. - Atmos., 115, https://doi.org/10.1029/2010JD014437, 2010.

Nuijens, L., Stevens, B., and Siebesma, A. P.: The environment of precipitating shallow cumulus convection, J. Atmos. Sci., 66, 1962–1979, https://doi.org/10.1175/2008JAS2841.1, 2009.

Nuijens, L., Serikov, I., Hirsch, L., Lonitz, K., and Stevens, B.: The distribution and variability of low-level cloud in the North Atlantic trades, Q. J. Roy. Meteor. Soc., 140, 2364–2374, https://doi.org/10.1002/qj.2307, 2014.

Prospero, J. M. and Carlson, T. N.: Vertical and areal distribution of Saharan dust over the western equatorial north Atlantic Ocean, J. Geophys. Res, 77, 5255–5265, https://doi.org/10.1029/JC077i027p05255, 1972.

Prospero, J. M. and Lamb, P. J.: African droughts and dust transport to the Caribbean: climate change implications, Science, 302, 1024–1027, https://doi.org/10.1126/science.1089915, 2003.

Sakai, T., Nagai, T., Zaizen, Y., and Mano, Y.: Backscattering linear depolarization ratio measurements of mineral, sea-salt, and ammonium sulfate particles simulated in a laboratory chamber, Appl. Opt., 49, 4441, https://doi.org/10.1364/ao.49.004441, 2010.

Seifert, P., Ansmann, A., Mattis, I., Wandinger, U., Tesche, M., Engelmann, R., Müller, D., Pérez, C., and Haustein, K.: Saharan dust and heterogeneous ice formation: Eleven years of cloud observations at a central European EARLINET site, J. Geophys. Res., 115, https://doi.org/10.1029/2009jd013222, 2010.

Stein, A. F., Draxler, R. R., Rolph, G. D., Stunder, B. J. B., Cohen, M. D., and Ngan, F.: NOAA's HYSPLIT atmospheric transport and dispersion modeling system, B. Am. Meteorol. Soc., 96, 2059–2077, https://doi.org/10.1175/BAMS-D-14-00110.1, 2015.

Stephens, G. L., Vane, D. G., Boain, R. J., Mace, G. G., Sassen, K., Wang, Z., Illingworth, A. J., O'Connor, E. J., Rossow, W. B., Durden, S. L., Miller, S. D., Austin, R. T., Benedetti, A., Mitrescu, C., and the CloudSat Science Team.: The CloudSat Mission and the A-Train, B. Am. Meteorol.. Soc., 83, 1771–1790, https://doi.org/10.1175/BAMS-83-12-1771, 2002.

Stephens, G. L., Wood, N. B., and Pakula, L. A.: On the radiative effects of dust on tropical convection, Geophys. Res. Lett., 31, https://doi.org/10.1029/2004gl021342, 2004.

Stevens, B., Ament, F., Bony, S., Crewell, S., Groß, S., Hirsch, L., Mayer, B., Wendisch, M., Wirth, M., Bakan, S., Brück, H.-M., Ehrlich, A., Ewald, F., Farell, D., Forde, M., Gödde, F., Grob, H., Hagen, M., Hansen, A., Jacob, M., Jäkel, E., Jansen, F., Klepp, C., Klingenbiel, M., Kölling, T., Konow, H., Mech, M., Peters, G., Rapp, M., Wing, A., and Wolf, K.: A high-altitude long-range aircraft configured as a cloud observatory - the NARVAL expeditions, B. Am. Meteorol. Soc., 2018, submitted.

Tesche, M., Ansmann, A., Müller, D., Althausen, D., Mattis, I., Heese, B., Freudenthaler, V., Wiegner, M., Esselborn, M., Pisani, G., and Knippertz, P.: Vertical profiling of Saharan dust with Raman lidars and airborne HSRL in southern Morocco during SAMUM, Tellus B, 61, 144–164, https://doi.org/10.1111/j.1600-0889.2008.00390.x, 2009.

Weinzierl, B., Ansmann, A., Prospero, J. M., Althausen, D., Benker, N., Chouza, F., Dollner, M., Farrell, D., Fomba, W. K., Freudenthaler, V., Gasteiger, J., Groß, S., Haarig, M., Heinold, B., Kandler, K., Kristensen, T. B., Mayol-Bracero, O. L., Müller, T., Reitebuch, O., Sauer, D., Schäfler, A., Schepanski, K., Spanu, A., Tegen, I., Toledano, C., and Walser, A.: The Saharan Aerosol Long-Range Transport and Aerosol-Cloud-Interaction Experiment: overview and selected highlights, B. Am. Meteorol. Soc., 98, 1427–1451, https://doi.org/10.1175/BAMS-D-15-00142.1, 2017.

Wendisch, M., Müller, D., Schell, D., and Heintzenberg, J.: An Airborne Spectral Albedometer with Active Horizontal Stabilization, J. Atmos. Ocean. Tech., 18, 1856–1866, https://doi.org/10.1175/1520-0426(2001)018<1856:aasawa>2.0.co;2, 2001.

Wiegner, M., Groß, S., Freudenthaler, V., Schnell, F., and Gasteiger, J.: The May/June 2008 Saharan dust event over Munich: Intensive aerosol parameters from lidar measurements, J. Geophys. Res. - Atmos., 116, https://doi.org/10.1029/2011jd016619, 2011.

Winker, D. M., Pelon, J., Coakley, J. A., Ackerman, S. A., Charlson, R. J., Colarco, P. R., Flamant, P., Fu, Q., Hoff, R. M., Kittaka, C., Kubar, T. L., Le Treut, H., McCormick, M. P., Mégie, G., Poole, L., Powell, K., Trepte, C., Vaughan, M. A., and Wielicki, B. A.: The CALIPSO mission: A global 3D view of aerosols and clouds, B. Am. Meteorol. Soc., 91, 1211–1229, https://doi.org/10.1175/2010BAMS3009.1, 2010.

Wirth, M., Fix, A., Mahnke, P., Schwarzer, H., Schrandt, F., and Ehret, G.: The airborne multi-wavelength water vapor differential absorption lidar WALES: system design and performance, Appl. Phys. B, 96, 201–213, https://doi.org/10.1007/s00340-009-3365-7, 2009.

Wong, S. and Dessler, A. E.: Suppression of deep convection over the tropical North Atlantic by the Saharan air layer, Geophys. Res. Lett., 32, https://doi.org/10.1029/2004gl022295, 2005.

Wong, S., Colarco, P. R., and Dessler, A. E.: Principal component analysis of the evolution of the Saharan air layer and dust transport: comparisons between a model simulation and MODIS and AIRS retrievals, J. Geophys. Res.-Atmos., 111, https://doi.org/10.1029/2006JD007093, 2006.